2018 IEEE-RAS 18th International Conference on Humanoid Robots (Humanoids)
Beijing, China, November 6-9, 2018

Online 3D CoM Trajectory Generation for Multi-Contact Locomotion Synchronizing Contact

Mitsuharu Morisawa[1,*], Rafael Cisneros[1], Mehdi Benallegue[1],
Iori Kumagai[1], Adrien Escande[2], Fumio Kanehiro[1]

Abstract— **This paper proposes a fast computation method for 3D multi-contact locomotion. The contributions of this paper are (a) the derivation of the prospect centroidal dynamics by introducing a force distribution ratio, where the centroidal dynamics in multi-contact can be represented with a formulation similar to the inverted pendulum's one, and (b) the development of a fast computation method for generating a 3D center of mass (CoM) trajectory. The proposed method allows to generate a trajectory sequentially and to change the locomotion parameters at any time even under variable CoM height. Then, the contact timing of each end-effector can be adjusted to synchronize with the actual contact with the environment by shortening or extending the desired duration of the support phase. This can be used to improve the robustness of the locomotion. In this paper, we deal with a multi-contact locomotion which can be fully received a vertical reaction force from the environment and the validity of the proposed method is confirmed by several numerical results: the CoM motion while changing the contact timing and a multi-contact locomotion considering a transition between biped and quadruped walking in a dynamics simulator.**

I. Introduction

Humanoid robots are expected to work on demanding or hazardous tasks to reduce human's burden. Multi-contact locomotion has a large potential to improve the locomotion performance to get over a narrow/complicated environment. If the robot can freely contact the environment with any limbs, the reachable area will be further expanded. Figure 1 illustrates an example of multi-contact locomotion on uneven terrain where biped walking alone is difficult, but using the arms provides a feasible solution. Since it is difficult to accurately measure such environments, the ability to tolerate such unknown errors for multi-contact locomotion is required to improve stability. From the point of view of robust multi-contact locomotion, the main key technologies can be categorized as (a) CoM/Posture/Contact force control, which can be performed as tasks in a whole body control with several optimal approaches to distribute contact forces and joint torques, taking into account the physical limits and contact force constraints [1], [2]. In this case, the Divergent Component of Motion (DCM) [5], [6] or the Capture Point could be used for the CoM control [7], [8]. For instance, a dynamic gait transition between biped and quadruped locomotion without pause was realized based on the DCM, [5]. Using this approach, the global position control of each limb improves the robustness, for example when climbing a vertical ladder [14]. (b) Contact force transition is usually controlled throughout a future horizon as presented by Nagasaka et al. [3]. In this method, a feasible contact force trajectory can be generated by using Model Predictive Control (MPC). As a practical example, a feasible climbing ladder motion is generated from a sequence of collision-free key poses and a trajectory is interpolated by MPC under physical constraints, but it ran offline in [12]. As a simple way, Kajita proposed the ZMP tracking control which takes into account the time delay of the ZMP [4]. (c) Adaptive trajectory generation is needed to maintain balance against external forces or unexpected contacts by a modification of motion parameters such as contact position or motion duration. MPC also provides a general and a versatile framework for that [9], [11]. However, this control is still hard to be applied it to a closed loop control for multi-contact locomotion, mainly because of the increase in computational time when increasing the number of contact points, even for the most efficient developed algorithms.

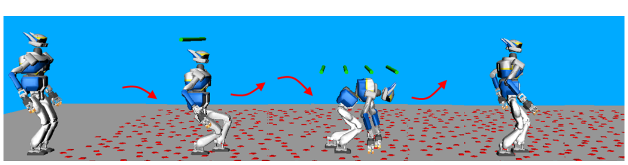

Fig. 1. Multi-contact locomotion with CoM up and down

[1]Humanoid Research Group, National Institute of Advanced Industrial Science and Technology (AIST), Tsukuba, Japan.
[2]CNRS-AIST JRL, UMI3218/RL, Tsukuba, Japan.
*Corresponding author E-mail: m.morisawa@aist.go.jp

In this paper, inspired by a fast 3D CoM trajectory generation focused on the DCM and proposed by Takenaka [13], [14], we extend to generate 3D CoM trajectory for multi-contact locomotion which can change the locomotion parameters at any time. In the previous method, the algorithm was mainly used to determine a last step in order to track the desired ZMP strictly and it did not achieve a modification of the parameters while walking. In Sec.II, we derive a good outlook formulation of the centroidal dynamics which is represented by a force distribution ratio. This formulation can prevent dramatic increases in computation time due to the number of contact points. Then, a low computation method of the 3D CoM trajectory generation and how to synchronize the contact timing will be explained in Sec.III. The generated trajectories are evaluated and a biped locomotion with variable height and a multi-contact motion are shown in Sec.IV.

II. Multi-Contact Centroidal Dynamics

A. Contact Constraint

The centroidal dynamics have been widely used as a description of the macroscopic behavior of the robot [3],

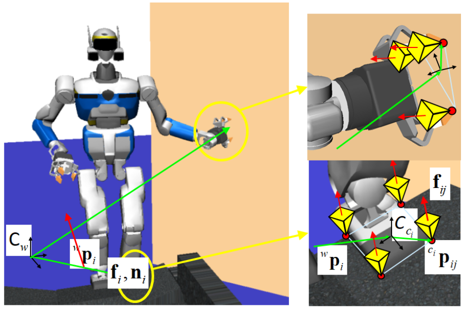

Fig. 2. Coordinates system

[7], [9]-[12], especially when it makes contact with the environment. The equations are:

$$\dot{\mathcal{P}} = \sum_{i=1}^{L} \boldsymbol{f}_i + m\boldsymbol{g}, \tag{1}$$

$$\dot{\mathcal{L}} = \sum_{i=1}^{L} \{(\boldsymbol{p}_i - \boldsymbol{p}_G) \times \boldsymbol{f}_i + \boldsymbol{n}_i\}, \tag{2}$$

where $\mathcal{P}(= m\dot{\boldsymbol{p}}_G) \in \mathbb{R}^3$ and $\mathcal{L} \in \mathbb{R}^3$ are the linear and the angular momentums around the CoM respectively. $\boldsymbol{p}_G \in \mathbb{R}^3$ is the CoM position, m is the total mass of the robot, and $\boldsymbol{g} = [0\ 0\ -g]^T$ is the gravity vector. $\boldsymbol{p}_i \in \mathbb{R}^3$ is the i-th contact position, L is the number of contact links, and $\boldsymbol{f}_i \in \mathbb{R}^3$ and $\boldsymbol{n}_i \in \mathbb{R}^3$ are the i-th contact force and torque. Substituting (1) into (2), the centroidal dynamics can be rewritten as

$$\begin{bmatrix} m\boldsymbol{I}_3 & \boldsymbol{0} \\ m\,[\boldsymbol{p}_G\times] & \boldsymbol{I}_3 \end{bmatrix} \begin{bmatrix} \ddot{\boldsymbol{p}}_G \\ \dot{\mathcal{L}} \end{bmatrix} + \begin{bmatrix} m\boldsymbol{g} \\ m\boldsymbol{p}_G \times \boldsymbol{g} \end{bmatrix} = \begin{bmatrix} \boldsymbol{f}_o \\ \boldsymbol{n}_o \end{bmatrix}, \tag{3}$$

where $[\boldsymbol{x}\times]$ generates a skew symmetric matrix from a vector $\boldsymbol{x} \in \mathbb{R}^3$, and $\boldsymbol{f}_o$,$\boldsymbol{n}_o \in \mathbb{R}^3$ are the reaction force and torque in the world coordinates respectively. A contact pair between the humanoid robot and the environment can be expressed as a set of points, as shown in Fig. 2. Let us suppose a contact surface between the i-th link frame and the environment. The j-th contact position expressed in the i-th local frame $\mathcal{C}_{c_i}$ is denoted as ${}^{c_i}\boldsymbol{p}_j$. If $\boldsymbol{p}_i$ is the position of the i-th link expressed in world coordinates $\mathcal{C}_w$, then for each contact position we have

$$\boldsymbol{p}_{ij} = \boldsymbol{p}_i + \boldsymbol{R}_{c_i}{}^{c_i}\boldsymbol{p}_j, \tag{4}$$

where $\boldsymbol{R}_{c_i}$ is the rotation matrix from the local frame to the world frame. The contact wrench in (3) is represented as

$$\begin{bmatrix} \boldsymbol{f}_o \\ \boldsymbol{n}_o \end{bmatrix} = \sum_{i=1}^{L}\sum_{j=1}^{M_i} \begin{bmatrix} \boldsymbol{f}_{ij} \\ \boldsymbol{p}_{ij} \times \boldsymbol{f}_{ij} \end{bmatrix}. \tag{5}$$

M_i is number of contact points at each link. Now, a polyhedral approximation of the friction cone is applied to each contact position, as it has been widely used in [3], [7], [9]-[11], [16]. We denote as $\boldsymbol{e}_{ijk}$ the k-th ray generating the polyhedral cone associated to $\boldsymbol{f}_{ij}$. Then $\boldsymbol{f}_{ij}$ can be written as

$$\boldsymbol{f}_{ij} = \sum_{k=1}^{N_j} \boldsymbol{f}_{ijk} = \sum_{k=1}^{N_j} \lambda_{ijk}\boldsymbol{e}_{ijk}, \ \ \lambda_{ijk} \geq 0, \tag{6}$$

where N_j is the number of edges of the pyramidal approximation of the cone, and $\lambda_{ijk} \geq 0$ expresses the unilateral nature of the contact. In this paper, we take $N_j = 4$ (4-sided pyramid) for all contact points. From (6), we get for each contact point that

$$\begin{aligned} \begin{bmatrix} \boldsymbol{f}_{ij} \\ \boldsymbol{n}_{ij} \end{bmatrix} &= \begin{bmatrix} \boldsymbol{e}_{ij1} & \cdots & \boldsymbol{e}_{ijN_j} \\ \boldsymbol{p}_{ij} \times \boldsymbol{e}_{ij1} & \cdots & \boldsymbol{p}_{ij} \times \boldsymbol{e}_{ijN_j} \end{bmatrix} \boldsymbol{\lambda}_{ij} \\ \boldsymbol{\lambda}_{ij} &\stackrel{\text{def}}{=} \begin{bmatrix} \lambda_{ij1}, & \cdots, & \lambda_{ijN_j} \end{bmatrix}^T \geq \boldsymbol{0} \end{aligned} \tag{7}$$

B. Representation by Force Distribution Ratio

Generally, the centroidal dynamics have been used in a whole-body task space controller as a dynamical equality constraint [2], [7], [10]. For the robustness of the locomotion, it is necessary to change a contact position and its timing when the robot loses balance. Although MPC algorithms for a multi-contact locomotion have been developed [3], [9], [11], [12], they are only used to generate a dynamically feasible offline motion and it is still hard to handle a short step period. In this paper, we formulate the centroidal dynamics by using a force distribution ratio between all contact links. This helps to generate the CoM motion intuitively. Instead of a contact constraint in (7), the contact wrench $\boldsymbol{f}_i$ and $\boldsymbol{n}_i$ of each link in contact is used:

$$\begin{bmatrix} \boldsymbol{f}_i \\ \boldsymbol{n}_i \end{bmatrix} = \sum_{j=1}^{M_i} \begin{bmatrix} \boldsymbol{f}_{ij} \\ \boldsymbol{p}_{ij} \times \boldsymbol{f}_{ij} \end{bmatrix} \tag{8}$$

Using (8), the contact wrench of the centroidal dynamics (5) becomes

$$\begin{aligned} \begin{bmatrix} \boldsymbol{f}_o \\ \boldsymbol{n}_o \end{bmatrix} &= \sum_{i=1}^{L} \begin{bmatrix} \boldsymbol{f}_i \\ \boldsymbol{p}_i \times \boldsymbol{f}_i + \boldsymbol{n}_i \end{bmatrix} \\ &= \begin{bmatrix} \boldsymbol{J}_t \\ \boldsymbol{J}_r \end{bmatrix} \boldsymbol{f}_c + \begin{bmatrix} \boldsymbol{0} \\ \boldsymbol{J}_t \end{bmatrix} \boldsymbol{n}_c \end{aligned} \tag{9}$$

where $\boldsymbol{f}_c = [\boldsymbol{f}_1^T \ \cdots \boldsymbol{f}_L^T]^T \in \mathbb{R}^{3L}$ and $\boldsymbol{n}_c = [\boldsymbol{n}_1^T \ \cdots \boldsymbol{n}_L^T]^T \in \mathbb{R}^{3L}$ are the sets of contact forces and torques of each link, $\boldsymbol{J}_t \in \mathbb{R}^{3\times 3L}$ and $\boldsymbol{J}_r \in \mathbb{R}^{3\times 3L}$ are the contact Jacobians. From the upper part of (9), the contact force can be obtained as

$$\boldsymbol{f}_c = \boldsymbol{J}_t^{+}(m(\ddot{\boldsymbol{p}}_G + \boldsymbol{g})) + (\boldsymbol{I}_{3L} - \boldsymbol{J}_t^{+}\boldsymbol{J}_t)\boldsymbol{f}_{int}, \tag{10}$$

where $\boldsymbol{J}_t^{+} = \boldsymbol{W}\boldsymbol{J}_t^T(\boldsymbol{J}_t\boldsymbol{W}\boldsymbol{J}_t^T)^{-1}$ is the weighted Moore-Penrose pseudo inverse matrix[1] and $\boldsymbol{f}_{int} \in \mathbb{R}^{3L}$ represents the internal force. The weight matrix is set to diagonal with $\boldsymbol{W} = diag\{w_{x1}, w_{y1}, w_{z1}, \cdots, w_{xL}, w_{yL}, w_{zL}\} \in \mathbb{R}^{3L\times 3L}$ and $w_{ij} \geq 0$. The pseudo inverse matrix of (10) can be analytically calculated as

$$\boldsymbol{J}_t^{+} = \begin{bmatrix} \boldsymbol{\alpha}_1 & \cdots & \boldsymbol{\alpha}_L \end{bmatrix}^T, \tag{11}$$

where

$$\begin{aligned} \boldsymbol{\alpha}_i &= diag\{\alpha_{xi}, \alpha_{yi}, \alpha_{zi}\} \in \mathbb{R}^{3\times 3}, \\ &= diag\left\{ \frac{w_{xi}}{\sum_{i=1}^{L} w_{xi}}, \frac{w_{yi}}{\sum_{i=1}^{L} w_{yi}}, \frac{w_{zi}}{\sum_{i=1}^{L} w_{zi}} \right\} \end{aligned} \tag{12}$$

[1] We describe $\boldsymbol{W}$ instead of $\boldsymbol{W}^{-1}$

From (12), the sum of weight in each axis obviously becomes

$$\sum_{i=1}^{L} \alpha_{xi} = \sum_{i=1}^{L} \alpha_{yi} = \sum_{i=1}^{L} \alpha_{zi} = 1. \tag{13}$$

Let us denote $\alpha_{\circ i}$ as a force distribution ratio for the CoM motion. We represent a force distribution by a time polynomial function to realize an appropriate force transition. From (3), (9) and (10), the angular momentum rate of the centroidal dynamics can be expressed as

$$\begin{aligned} &\left([\boldsymbol{p}_G\times] - \sum_{i=1}^{L}[\boldsymbol{p}_i\times]\boldsymbol{\alpha}_i\right)\ddot{\boldsymbol{p}}_G \\ &= \; -\left([\boldsymbol{p}_G\times] - \sum_{i=1}^{L}[\boldsymbol{p}_i\times]\boldsymbol{\alpha}_i\right)\boldsymbol{g} - \frac{\boldsymbol{\sigma}}{m}, \end{aligned} \tag{14}$$

where

$$\boldsymbol{\sigma} \;=\; -\dot{\boldsymbol{\mathcal{L}}} + \boldsymbol{J}_r(\boldsymbol{I}_{3L} - \boldsymbol{J}_t^{+}\boldsymbol{J}_t)\boldsymbol{f}_{int} + \boldsymbol{n}_c \tag{15}$$

In case of non flat plane, the internal force affects the inertial CoM motion through the nullspace projection matrix in the second term of the right side of (10). By extracting the horizontal CoM motion, (14) can be represented as

$$\begin{aligned} \ddot{x}_G &= \frac{g+\ddot{z}_G}{z_G - \sum_{i=1}^{L}\alpha_{xi}p_{zi}} \left(x_G - \sum_{i=1}^{L}\alpha_{zi}p_{xi} + \frac{\sigma_y}{m(g+\ddot{z}_G)}\right), \\ \ddot{y}_G &= \frac{g+\ddot{z}_G}{z_G - \sum_{i=1}^{L}\alpha_{yi}p_{zi}} \left(y_G - \sum_{i=1}^{L}\alpha_{zi}p_{yi} - \frac{\sigma_x}{m(g+\ddot{z}_G)}\right), \end{aligned} \tag{16}$$

where $\sum_{i=1}^{L}\alpha_{xi}p_{zi}$ and $\sum_{i=1}^{L}\alpha_{yi}p_{zi}$ encode the virtual height via $z_h = z_G - \sum_{i=1}^{L}\alpha_{\circ i}p_{zi} (\circ = x, y)$, i.e. the denominator mentioned above is the pendulum height. When the virtual height is higher than the CoM height, the CoM behaves as a non-inverted pendulum. $\sum_{i=1}^{L}\alpha_{zi}p_{xi}$ and $\sum_{i=1}^{L}\alpha_{zi}p_{yi}$ consist of the representative contact point and the other term which is the derivative of the angular momentum and related to the contact force on a non-flat surface. When the contact positions allow force closure, the CoM can be moved in any direction [16].

III. Online CoM Trajectory Generation for Multi-Contact

As a way to improve the adaptability of locomotion, the CoM trajectory can be generated in synchronization with the contacts with the environment. When the desired contact position and timing are preplanned, it is necessary to generate multi-contact locomotion sequentially so that the timing or contact position can be immediately changed. In this section, we propose a very fast computation method of the CoM trajectory under this dynamics. From the basic concept in [8], [19], the trajectory generation is composed of 2 terms: a *long* and a *short term trajectory*.

A. Long term trajectory of the CoM

In a similar way to [5], the discretized system of the centroidal dynamics in the sagittal plane of (16) with a sampling period ΔT can be obtained as

$$\boldsymbol{x}_{k+1} \;=\; \boldsymbol{A}_k\boldsymbol{x}_k + \boldsymbol{B}_k u_k, \tag{17}$$

where,

$$\begin{aligned} \boldsymbol{x}_k &= \begin{bmatrix} x_{G,k} \\ \dot{x}_{G,k} \end{bmatrix}, u_k = \sum_{i=1}^{L}\alpha_{zi,k}p_{xi,k} - \frac{\sigma_{y,k}}{m(g+\ddot{z}_{G,k})}, \\ \boldsymbol{A}_k &= \begin{bmatrix} \cosh(\omega_k\Delta T) & \frac{\sinh(\omega_k\Delta T)}{\omega_k} \\ \omega_k\sinh(\omega_k\Delta T) & \cosh(\omega_k\Delta T) \end{bmatrix}, \\ \boldsymbol{B}_k &= \begin{bmatrix} 1-\cosh(\omega_k\Delta T) \\ -\omega_k\sinh(\omega_k\Delta T) \end{bmatrix}, \\ \omega_k &= \sqrt{\frac{g+\ddot{z}_{G,k}}{z_{G,k} - \sum_{i=1}^{L}\alpha_{xi,k}p_{zi,k}}}. \end{aligned} \tag{18}$$

where $\boldsymbol{u}_k$ is equivalent to the ZMP[2]. This equation becomes a Linear Time-Varying System (LTVS) under a variable height of the CoM, the angular momentum rate, a varying force distribution ratio, and an internal force. The CoM motion in the frontal plane can be also discussed as the same way as in the sagittal plane (18). When the future sequence of a contact position, a force transition and also the angular momentum rate are preplanned, the future input of u_k will be given. The CoM state $\boldsymbol{x}_F$ after the F-th future step is

$$\boldsymbol{x}_F = \boldsymbol{\Phi}(F,0)\boldsymbol{x}_0 + \sum_{i=0}^{F-1}\boldsymbol{\Phi}(F,i+1)\boldsymbol{B}_i u_i \tag{19}$$

where,

$$\boldsymbol{\Phi}(k,j) = \begin{cases} \boldsymbol{A}_{k-1}\boldsymbol{A}_{k-2}\cdots\boldsymbol{A}_j & \text{if } k > j \\ \boldsymbol{I}_2 & \text{otherwise } (k=j=F) \end{cases}$$

Generally in order to generate a smooth trajectory sequentially, the boundary condition as the CoM position and velocity also the ZMP position should be satisfied. Furthermore, an input u as a representative center of pressure is also restricted under the physical contact condition. This input causes a variation to accelerate/decelerate the CoM when starting/stopping the locomotion, or when changing it. Therefore the computational cost to find an optimal input u under these constraints becomes high.

In the case of MPC, the trajectory can be generated as a QP problem which is solved to find a set of inputs $u_0 \cdots u_F$ such that the generated trajectory can track the desired one. In the calculation process for LTVS, one has to solve a system of linear equations with a number of variables proportional to the length of preview window divided by the sampling period. In this paper, we introduce a simple boundary condition to calculate the long term trajectory online. In order to reduce the variation of the input, we calculate a trajectory from past contact parameters. Instead of the preview window going from the current step 0 to the future step F in (19), we

[2] More exactly, this is named as the Centroidal Momentum Pivod (CMP) with $\dot{\mathcal{L}}_x \neq 0$, and $\dot{\mathcal{L}}_y \neq 0$ [17]

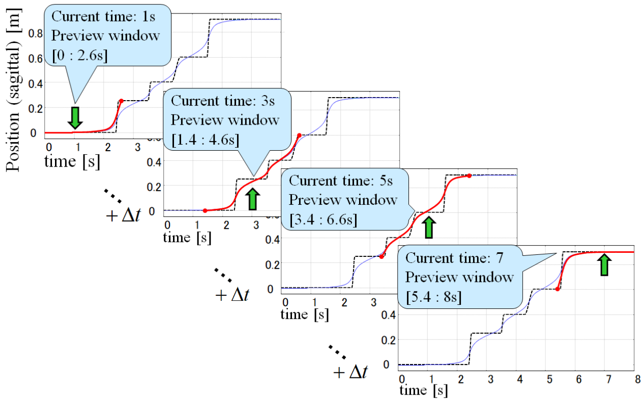

Fig. 3. Sequential trajectory generation from past to future

adopt a preview window going from a past step $P < 0$ to the future step F. In fact, P can be set to $-F$. This trajectory can be generated sequentially at every sampling period shown in Fig.3. Note that the continuity of this trajectory is not guaranteed. The continuity can be guaranteed by the short term trajectory described in Sec. III-B. As we can see in Fig.3, the state difference calculated from the previous and the current step, becomes very small by calculating from the past. This compensation value will get almost 0 during locomotion unless the locomotion parameters are changed. The computational cost doubles because the length of the preview window doubles. However, since the size of the matrix is 2×2, the computational cost is much smaller than MPCs. Then (19) can be represented as

$$\begin{bmatrix} x_F \\ \dot{x}_F \end{bmatrix} = \underbrace{\begin{bmatrix} a_{11} & a_{12} \\ a_{21} & a_{22} \end{bmatrix}}_{\mathbf{\Phi}(F,P)} \begin{bmatrix} x_P \\ \dot{x}_P \end{bmatrix} + \underbrace{\begin{bmatrix} b_1 \\ b_2 \end{bmatrix}}_{\sum_{i=P}^{F-1} \mathbf{\Phi}(F,i+1)\boldsymbol{B}_i u_i}. \quad (20)$$

When we set the initial and the terminal CoM position to the same value of input u_k as

$$x_P = u_P, \ x_F = u_F,$$

the CoM trajectory can be calculated without modification of the input. Reconstructing (20), the initial and the terminal velocity of the CoM can be obtained as

$$\begin{bmatrix} \dot{x}_P \\ \dot{x}_F \end{bmatrix} = \frac{1}{a_{12}} \begin{bmatrix} -1 & 0 \\ -a_{22} & a_{12} \end{bmatrix} \times \left(\begin{bmatrix} a_{11} & -1 \\ a_{21} & 0 \end{bmatrix} \begin{bmatrix} x_P \\ x_F \end{bmatrix} + \begin{bmatrix} b_1 \\ b_2 \end{bmatrix} \right). \quad (21)$$

Finally, the next state can be calculated as

$$\boldsymbol{x}_1^{lg} = \mathbf{\Phi}(1,P)\boldsymbol{x}_P + \sum_{i=P}^{1} \mathbf{\Phi}(1,i+1)\boldsymbol{B}_i u_i. \quad (22)$$

The long term trajectory of LTVS can be calculated uniquely without any tuning of parameters.

B. Short term trajectory of the CoM

A short term trajectory is generated to smoothly follow a long term trajectory with the discontinuities mainly caused by the change of a contact position or a contact timing. We adopt the variations of the CoM position, velocity and the equivallent ZMP position from the long term trajectory as state variables for this purpose. The extended system of (17) is available by considering differentiation of u as an input. The system equation can be represented as

$$\boldsymbol{x}_{t+1} = \boldsymbol{A}_t \boldsymbol{x}_t + \boldsymbol{B}_t \dot{u}_t, \quad (23)$$

where

$$\begin{aligned} \boldsymbol{x}_t &= \begin{bmatrix} x_t & \dot{x}_t & u_t \end{bmatrix}^T, \\ \boldsymbol{A}_t &= \begin{bmatrix} \cosh(\omega_t \Delta T) & \frac{\sinh(\omega_t \Delta T)}{\omega_t} & 1-\cosh(\omega_t \Delta T) \\ \omega_t \sinh(\omega_t \Delta T) & \cosh(\omega_t \Delta T) & -\omega_t \sinh(\omega_t \Delta T) \\ 0 & 0 & 1 \end{bmatrix}, \\ \boldsymbol{B}_t &= \begin{bmatrix} 0 & 0 & \Delta T \end{bmatrix}^T, \end{aligned} \quad (24)$$

Then we apply a simple state feedback controller

$$\dot{u}_t = \boldsymbol{F}_t(\boldsymbol{x}^{ref} - \boldsymbol{x}_t), \quad (25)$$

into the system equation in (23). $\boldsymbol{x}^{ref} = [x_1^{lg} \ \dot{x}_1^{lg} \ u_1^{lg}]^T$ is the target reference which is updated from the long term trajectory as the next desired state in (22) ($u_1^{lg} = u_1$). Then, the closed loop system becomes

$$\boldsymbol{x}_{t+1} = (\boldsymbol{A}_t - \boldsymbol{B}_t \boldsymbol{F}_t)\boldsymbol{x}_t. \quad (26)$$

In this paper, we suppose LTVS to be constant during each sampling time and design the feedback gain by pole assignment. In our knowledge, the good tracking performance can be obtained by placing one of the eigenvalues of the characteristic equation of (26) at 0 and the remaining two eivenvalues close to 1. A example of the generated CoM and ZMP trajectories is shown in Fig. 4. Here, we assign the eigenvalues of the closed loop system to $(0.015, 0.985, 0.985)$. In order to follow the long term trajectory, the ZMP overshoot of the short term trajectory has occured (Fig. 4 (a)). However, this will be small enough when the locomotion parameters are not changed within the preview time (Fig. 4 (b)).

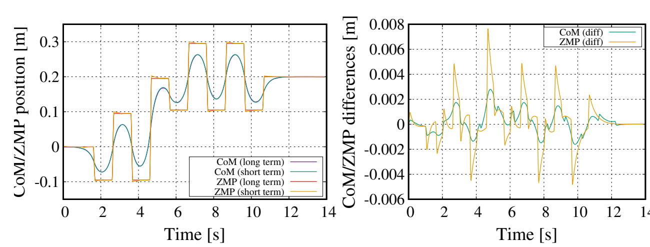

(a) Long and short term trajetories (b) Difference between long and short term trajectory

Fig. 4. Example of the generated trajectory

Computation costs according to the number of the future and the past preview step $F(= P)$ used to generate a 3D CoM trajectory are shown in Fig.5. In the MPC, the computation time increases in proportion to the square of the preview size, but this algorithm is simply proportional. The preview time is $T_p = F \times \Delta T$. The CoM trajectory is generated from $-T_P$ to T_P. This includes the horizontal trajectory of the CoM (twice of the long and the short term) and the CoM height with 3rd time polynomial interpolation. We run the algorithm on an Intel(R) Core(TM) i7-4900MQ CPU 2.80GHz. For instance, as we set the preview time to 1.6s with 5ms sampling time, F becomes 320. In this preview size, the CoM trajectory can be calculated in $60\mu s$.

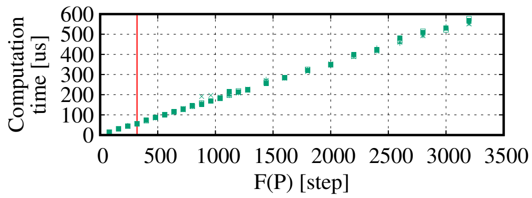

Fig. 5. Computation costs according to the preview step $F(=P)$

C. Contact Timing Adjustment

Although a small error of the ground information can be absorbed by compliance of the end-effectors, the robot can easily lose balance on uneven floor. To improve the stability, we consider to generate the CoM/ZMP trajectories synchronized with the contacts on the ground. At the swing phase of each end-effector, the trajectories are generated so that the period

$$T_{swing} = \begin{cases} T_{current} & \text{if contact is detected} \\ T_{swing} + \Delta T & \text{otherwise} \end{cases},$$

can be shortened or extended according to the detection of a contact force. If a contact force is not detected until the maximum permissible time, a period of the swing phase is increased by one sampling period ($\Delta T = 5$[ms]). Then, the swing support passes to the next phase after a contact force detection or after reaching the maximum value. We set an acceptable landing time, and the end-effector will get down with a constant speed during that period. The waist height at a next step is updated to a weighted average of the difference between the desired and the actual landing position which is used as the desired force distribution ratio. As a remark for the quadruped locomotion, if more than two end-effectors are moved, the algorithm waits for all of the contacts to be detected to go to the next phase.

D. Error analysis of the long term trajectory

If the ZMP is 0 during all periods, the position of the CoM also should be 0. Therefore, a maximum error of the long term CoM trajectory will be caused when the ZMP is largely changed only at the boundary of the preview time. Figure 6 (a) shows an example of the CoM trajectory when the boundary ZMP positions are set to $(-0.1 \rightarrow \pm 0.1m)$, $(-0.3 \rightarrow \pm 0.3m)$, $(-0.5 \rightarrow \pm 0.5m)$, and $(-0.7 \rightarrow \pm 0.7m)$ at $t = [-1.6 : 1.6](s)$ respectively and are set to 0 the rest of time. Future and past preview times are set to 1.6s respectively, i.e. 0s means current time. We use a constant CoM height of 0.8m. In Fig.6 (b), an enlarged view of (a), we can see that the generated ZMP becomes smaller than 0.01m at 0s even if the future ZMP is set at any range of $[-0.7 : 0.7](m)$ at 1.6s.

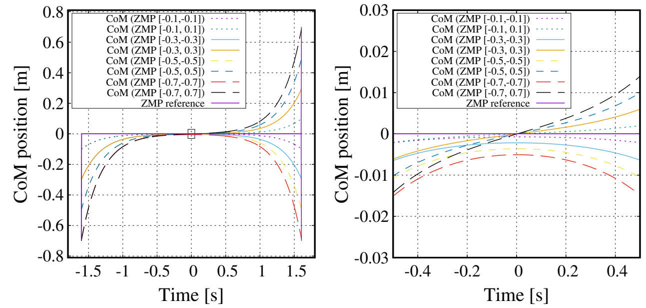

(a) CoM trajectory (b) Enlarged view of (a)

Fig. 6. CoM trajectory during preview window

Next, let us derive this maximum error of the CoM analytically. From a formulation similar to (17), a time response of the CoM can be represented as

$$\begin{bmatrix} x_f \\ \dot{x}_f \end{bmatrix} = \begin{bmatrix} \cosh(\omega t) & \frac{\sinh(\omega t)}{\omega} \\ \omega \sinh(\omega t) & \cosh(\omega t) \end{bmatrix} \begin{bmatrix} x_i \\ \dot{x}_i \end{bmatrix} + \begin{bmatrix} 1 - \cosh(\omega t) \\ -\omega \sinh(\omega t) \end{bmatrix} u, \qquad (27)$$

where x_i and x_f are the initial and the final position of the CoM, and u is the ZMP position. Now we consider the CoM motion during a past and a future preview time, i.e. $x_i = x(-T_p), x_f = x(T_p), t \in [-T_p : T_p]$ are set as the boundary conditions. From Fig.6, the CoM error can be maximized when the initial and the final positions of the CoM are the same $(x(-T_p) = x(T_p))$. That is the CoM trajectory becomes a symmetric motion around the current time. The final velocity of the CoM should have the opposite sign of the initial velocity: $(\dot{x}(-T_p) = -\dot{x}(T_p))$. Then, the CoM error can be obtained as the CoM position at $t = 0$.

$$x_{err} = \underbrace{\left(\cosh(\omega T_p) - \frac{\sinh(\omega T_p)\sinh(2\omega T_p)}{1 + \cosh(2\omega T_p)} \right)}_{CoM\ error\ ratio} x(T_p) \qquad (28)$$

Here, the CoM error becomes a function of the preview time T_p. We can also notice that the CoM error is proportional to the final/initial CoM position. Thus we can say "*CoM error ratio*" with respect to a future variation of the ZMP at this term. The relation between the CoM error ratio and the preview time is illustrated Fig. 7. Because it is

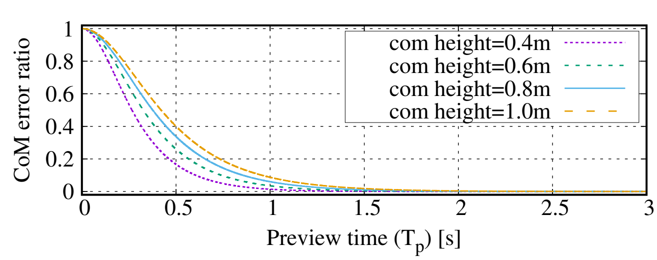

Fig. 7. Relation between CoM error ratio and preview time

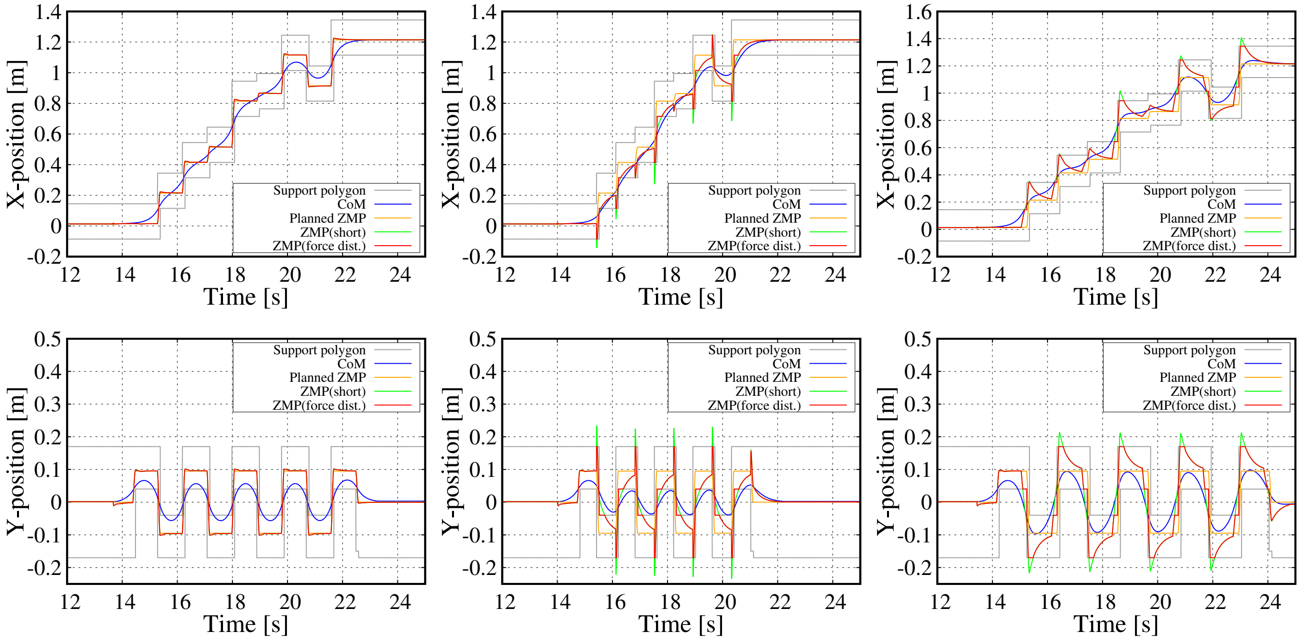

(a) Just expected contact (b) Early contact (c) Late contact

Fig. 8. CoM/ZMP trajectories (Top:Sagittal / Bottom:Frontal plane)

difficult to control the ZMP precisely, within 1cm in fact, and a step length will be set up to 1m, we can say that the CoM error ratio is sufficiently small if its ratio is less than 0.01. The preview times at which the CoM error ratio becomes smaller than 0.01 are 1.071s at 0.4m of the CoM height, 1.311s at 0.6m, 1.514s at 0.8m, and 1.693s at 1.0m respectively. Since the height of the CoM of our humanoid robot HRP-2KAI [20] at a standard posture is almost 0.8m, it is reasonable to set 1.6s as a preview time. In this regard, the CoM error, for which the trajectory is a combination of the long and short term trajectories, will be greater than this analytical error. This CoM error analysis is also available when the desired landing position is changed before a preview time.

IV. Simulation Results

A. Effectiveness of the contact timing adjustment

First, we evaluate the CoM / ZMP pattern generation of a biped walking motion with the contact timing adjustment offline. A contact detection signal from the ground is provided without dynamical simulation. We consider the support polygon so that the generated ZMP has to remain in this area. At force transition phase, force distribution ratio is interpolated by a 3rd order time polynomial. Figure 8 (a) shows the CoM and ZMP trajectories when every contact with the ground happens exactly at the planned timing. The ZMP trajectory provided by the pattern generation (i.e. short term trajectory) tracks the planned ZMP with small variations. We can see that the generated ZMP almost corresponds well to the planned ZMP as we explained in Sec. III-B. Figure 8 (b) shows the case where contact is detected before the preplanned contact timing. The duration of a single support is immediately reduced from 0.8s to 0.6s at 0.6s. In that case the preplanned contact timing shortens and shifts to the next force transition phase. The ZMP moves towards the opposite direction to CoM velocity leading to a CoM acceleration. Figure 8 (c) shows the situation when contacts are detected after a preplanned contact timing. Each single support phase is extended from 0.8s to 1.0s by increasing at every sampling period after 0.8s. In contrast with the case of an early contact, the ZMP overshoots in the direction of the CoM velocity and produces a deceleration of the CoM. In both cases, we can see that the ZMP goes out of the support region. Therefore, we need to modify the ZMP into a feasible one which satisfies the physical constraints. In this paper, the optimization-based force distribution is used to obtain the feasible ZMP reference.

B. Biped and Quadruped Locomotion on Uneven Terrain

To assess the stabilization performance of the 3D multi-contact locomotion by using the proposed method, we set up an uneven floor on which 1cm height blocks are scattered randomly. We also add a horizontal barrier at 1.6m height and 4 barriers at 1.2m height on the way of the robot. The robot goes under the first bar by bending the knees to lower the waist by 0.2m. The next four bars need to be passed under using quadruped locomotion. A control system extends our system [8] based on "LIPM tracking stabilization control" in [18] for a multi-contact locomotion. Each end-effector uses a damping controller in order to manipulate the contact force. This controller tracks the desired force and torque according to the force distribution ratio, then the joint angles are generated using a prioritized whole body inverse kinematics considering a limitation of joint angles, velocities, and self collision avoidance.

We prepared all of the contact positions, the desired

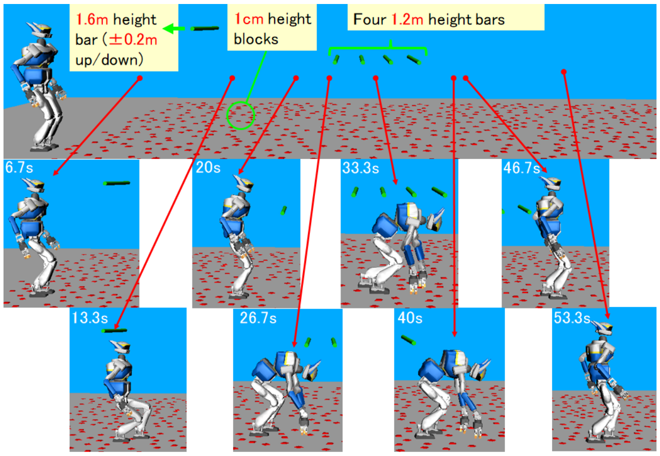

Fig. 9. Multi-contact locomotion on uneven terrain

contact timings and the variable waist height motion under an assumption of a flat floor without any environment recognition system. The preplanned step length and step cycle at steady state were set to 0.25m and 1.25s (0.9s single / 0.35s double support periods) for biped walking and 0.15m and 1.15s (0.9s 2-limbs / 0.25s 4-limbs support periods) for quadruped locomotion respectively. The support phase duration can be changed within a range of $\pm 0.2s$. The swing foot and hand approach the contact surface with a constant velocity -0.2m/s in the normal direction of the surface. The snapshots of the locomotion are displayed in Fig.9. We designed a contact state machine of quadruped locomotion as a "*trot*" gait. During quadruped locomotion, force distribution ratios of 40% and 60% were set to the hand and the foot during the 2-limbs support phase respectively. Half of these values were set to each hand and foot during the 4-limbs support phase.

The height of the CoM was determined from the position and orientation of the desired root link, assuming that the relative position between the root link and the CoM is constant. The priority of the position and orientation of the root link is set to lower than the position/orientation of the end-effectors. This approximation is accurate when the output of the waist height from the inverse kinematics is equal to the desired value. Figure 10 shows that the height of the waist produced by the prioritized inverse kinematics is different from the desired waist height during the quadruped locomotion at 45-63s. On the other hand, the 3D CoM is

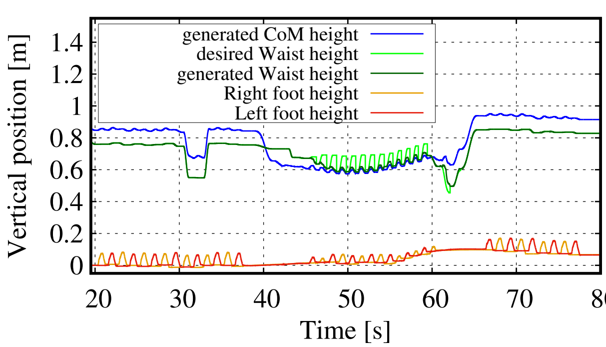

Fig. 10. Vertical trajectories of CoM/waist/feet

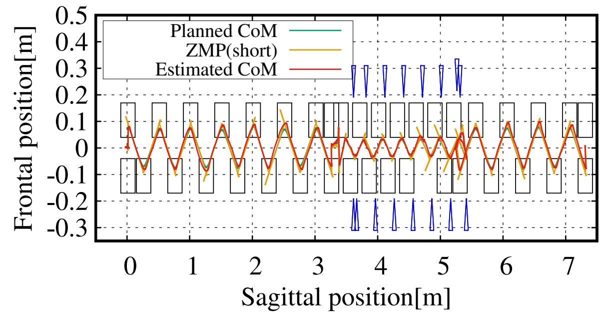

Fig. 11. Projection of horizontal CoM-ZMP trajectories on floor

tracking closely the reference, the differences are mostly due to modifications performed by the inverse kinematics. It is worth to note that the landing positions in this graph do not always correspond to the height of the terrain, this is because these positions are reconstructed using the kinematics which rely also on the attitude estimation. In particular, the landing error becomes larger when the robot stands up around 55-60s. This is mainly due to quick motions produced by the inverse kinematics in order to respect feasibility conditions such as self-collision avoidance.

The projection of the horizontal CoM-ZMP trajectories on the floor is shown in Fig.11. The rectangle and the triangle are the contact vertices of the sole and the fingers respectively. We can see that, using the proposed method, the CoM could track correctly the desired trajectory even on uneven terrain with variable heights of the CoM.

V. Conclusion

In this paper, we derived the centroidal dynamics in the case of multi-contact motion as a linear time variant system (LTVS) by introducing a force distribution ratio at each contact of the end-effectors. The force distribution ratio contributes to simplify the motion generation. Then we developed a fast computation method to generate variable height 3D CoM trajectories using the LTVS in order to update the CoM motion when the motion parameters (such as a landing time or position) are modified. The 3D CoM trajectory could be generated in $60\mu s$ at every step. The effectiveness of the proposed method was evaluated by a 3D CoM multi-contact locomotion synchronized with the actual contact with the environment by shortening or extending the desired duration of the support phase. Stable biped walks with variable waist height and transitions between biped and quadruped locomotion were realized.

In this paper, we dealt with multi-contact locomotion which can fully receive a vertical reaction force from the environment. This method can be applied in the case of shallow slopes. On the other hand, on a steep slope or a vertical wall, not only the force distribution rate but also the contact internal force contributes to the multi-contact locomotion. This is a problem that we can not deal with by using this approach. The method is unable to tackle the case of bilateral contacts like grasping handrail as well. Therefore, in the future work, we will extend the solution to these problems towards more general multi-contact situations.

ACKNOWLEDGMENT

This work was partially supported by NEDO's "Development of a highly dependable humanoid robot system that can work in unstructured environments" project and in part by the CNRS-AIST-Airbus Joint Research Program (JRP).

REFERENCES

[1] L. Sentis, J. Park, and O. Khatib, "Modeling and Control of Multi-Contact Centers of Pressure and Internal Forces in Humanoid Robots," *in Proc. of IEEE Int. Conf. on Robotics and Automation*, pp.453-460, 2009.

[2] B. Henze, A. Dietrich, and C. Ott, "An Approach to Combine Balancing with Hierarchical Whole-Body Control for Legged Humanoid Robots," *in IEEE Robotics and Automation Letters*, Vol.1, No.2, 2016.

[3] K. Nagasaka, T. Fukushima, and H. Shimomura, "Whole-body control of a humanoid robot based on generalized inverse dynamics and multi-contact stabilizer that can take account of contact constraints," *in Robotics Symposia* (in Japanese), Vol.17, 2012

[4] K. Miura, M. Morisawa, F. Kanehiro, S. Kajita, K. Kaneko and K. Yokoi, "Human-like Walking with Toe Supporting for Humanoids," *in Proc. of IEEE Int. Conf. on Intelligent Robots and Systems*, pp.4428-4435, 2011.

[5] T. Kamioka, T. Watabe, M. Kanazawa, H. Kaneko, and T. Yoshiike, "Dynamic Gait Transition between Bipedal and Quadrupedal Locomotion," *in Proc. of IEEE Int. Conf. on Intelligent Robots and Systems*, pp.2195-2201, 2015.

[6] J. Englsberger, C. Ott, and A. A-Schaffer, "Three-dimensional bipedal walking control based on divergent component of motion," *IEEE Transaction of Robotics*, Vol. 31, No. 2, pp.884-898, 2015.

[7] T. Koolen, S. Bertrand, G. Thomas, T. D. Boer T. Wu, J. Smith, J. Englsberger, and J. Pratt, "Design of a momentum-based control framework and application to the humanoid robot atlas," *in Int. Journal of Humanoid Robots*, Vol.13, No.1, p.1650007-1 - 1650007-34, 2016.

[8] M. Morisawa, N. Kita, S. Nakaoka, K. Kaneko, S. Kajita, and F. Kanehiro, "Biped locomotion control for uneven terrain with narrow support region," *in IEEE/SICE Int. Symposium on System Integration*, pp. 3439, 2014.

[9] H. Audren, J. Vaillant, A. Kheddar, A. Escande, K. Kaneko, and E. Yoshida, "Multi-contact Walking Pattern Generation based on Model Preview Control of 3D COM Accelerations," *in Proc. of IEEE Int. Conf. on Intelligent Robots and Systems*, pp.4030-4035, 2013.

[10] M. A. Hopkins, D. W. Hong, A. Leonessa, "Compliant Locomotion Using Whole-Body Control and Divergent Component of Motion Tracking," *in Proc. of IEEE Int. Conf. on Robotics and Automation*, pp.5726-5733, 2015.

[11] S. Caron and A. Kheddar, "Multi-contact Walking Pattern Generation based on Model Preview Control of 3D COM Accelerations," *in Proc. of IEEE Int. Conf. on Humanoid Robots*, pp.550-557, 2016.

[12] S. Nozawa, M. Kanazawa, Y. Kakiuchi, K. Okada, T. Yoshiike, and M. Inaba, "Three-dimensional Humanoid Motion Planning Using COM Feasible Region and its Application to Ladder Climbing Tasks," *in Proc. of IEEE Int. Conf. on Humanoid Robots*, pp.49-56, 2016.

[13] T. Takenaka, T. Matsumoto, T. Yoshiike, T. Hasegawa, S. Shirokura, H. Kaneko and A. Orita, "Real Time Motion Generation and Control for Biped Robot -4th Report: Integrated Balance Control-," *in Proc. of IEEE/RSJ Int. Conf. on Intelligent Robots and Systems*, pp.1601-1608, 2009.

[14] M. Kanazawa, S. Nozawa, Y. Kakiuchi, Y. Kanemoto, M. Kuroda, K. Okada, M. Inaba and T. Yoshiike, "Robust Vertical Ladder Climbing and Transitioning between Ladder and Catwalk for Humanoid Robots," *in Proc. of IEEE Int. Conf. on Intelligent Robots and Systems*, pp.2202-2209, 2015.

[15] A. D. Prete, S. Tonneau and N. Mansard, "Fast Algorithms to Test Robust static Equilibrium for Legged Robots," *in Proc. of IEEE Int. Conf. on Robotics and Automation*, pp.1601-1607, 2016.

[16] S. Caron, Q. Cuong and Y. Nakamura, "ZMP support areas for multi-contact mobility under frictional constraints," *IEEE Transaction of Robotics*, Vol. 33, Issue 1, pp.67-80, 2017.

[17] M. Popovic, A. Goswami and H. M. Herr, "Ground reference points in legged locomotion: definitions, biological trajectories and control implications," *Int. Journal of Robotics Research*, Vol.24, No.12, pp.1013-1032, 2005.

[18] S. Kajita, M. Morisawa, K. Miura, S. Nakaoka, K. Harada, K. Kaneko, F. Kanehiro, and K. Yokoi, "Biped walking stabilization based on linear inverted pendulum tracking," *in Proc. of IEEE/RSJ Int. Conf. on Intelligent Robots and Systems*, pp.4489-4496, 2010.

[19] M. Morisawa, F. Kanehiro, K. Kaneko, N. Mansard, J. Sola, E. Yoshida, K. Yokoi, and J-P. Laumond, "Combining Suppression of the Disturbance and Reactive Stepping for Recovering Balance," *in Proc. of IEEE Int. Conf. on Intelligent Robots and Systems*, pp.3150-3156, 2010.

[20] K. Kaneko, M. Morisawa, S. Kajita, S. Nakaoka, T. Sakaguchi, R. Cisneros, and F. Kanehiro, "Humanoid robot HRP-2 Kai - Improvement of HRP-2 towards disaster response tasks," *in Proc. of IEEE-RAS Int. Conf. on Humanoid Robots*, pp.132139, 2015.